

Adsorption and Sensing Mechanism of a $n\text{TiO}_2$ Particle ($n = 1-3$)-Doped MoTe_2 Monolayer to Faulty and Hazardous Gases in the Underground Cableway

Jipeng Mei* and Ziwen Yu

Cite This: *ACS Omega* 2024, 9, 17002–17011

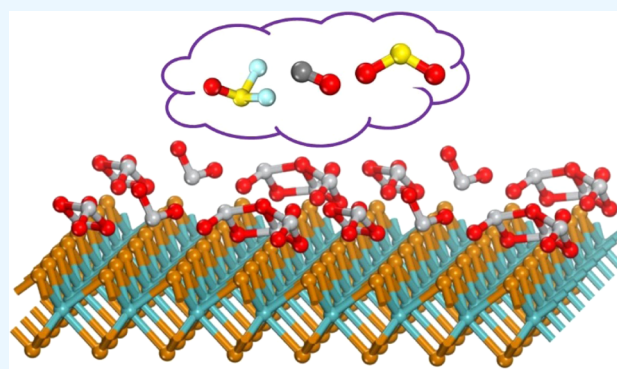
Read Online

ACCESS |

Metrics & More

Article Recommendations

ABSTRACT: With the rapid growth of the economy and industrial technology, vigorous and stable power distribution networks have gradually been established worldwide. Among these networks, underground cables play a crucial role in the distribution process, determining the overall electrical stability of entire cities. Based on density functional theory, this paper first proposes a TiO_2 particle-doped MoTe_2 monolayer to detect and eliminate these faults and hazardous gases within the underground cableway. The band structure, total density of states, projected density of states, and differential charge density are analyzed. The results demonstrate that the presence of TiO_2 particles significantly enhances the adsorption capacity of MoTe_2 , diminishes the electrical conductivity of the doping system, and heightens electron activity in the doping reaction zone. The best adsorption performance is achieved in the case of two-particle doping. Furthermore, the modified MoTe_2 exhibits an enhanced capability for capturing SO_2 and SOF_2 , with the adsorption mechanism classified as physical–chemical adsorption. This work not only introduces a novel surface modification method for a MoTe_2 monolayer but also provides a substantial data set to support the design and production of efficient sensors used in the underground cableway. These contributions further enhance the safety and stability of power systems and ensure human health.



1. INTRODUCTION

The safety concerns related to cable operation have consistently been a focal point within the high-voltage industry.^{1,2} They play a crucial role in determining power transmission across the entire region and serve as the lifeblood of the national economy. Nevertheless, in the present stage, the monitoring of cable faults significantly lags behind the rapid pace of technological advancement, resulting in numerous safety issues during production. One of these issues pertains to the inevitable development of insulation defects in the external insulation layer of cables as their operational lifespan increases, consequently leading to partial discharges (PDs).^{3,4} This process produces a substantial amount of fault gases and hazardous compounds, including CO , SO_2 , and SOF_2 . SO_2 is generated when cables are aged and heated, while the channel generates SOF_2 in the case of severe partial discharges. Meanwhile, the SF_6 gas contained in the cable insulation layer reacts with trace water under partial discharge conditions, generating various characteristic decomposition components such as SO_2 and SOF_2 at different concentrations.^{5,6} Simultaneously, as the discharge intensifies and the cable ages, a significant amount of CO will gradually be produced in underground cable channels.⁷ In addition, when a fire occurs in

the underground cableway, the insufficient combustion of the insulation also generates large amounts of CO . These gases not only pose a serious threat to the atmospheric environment but also present immeasurable risks to personnel working within underground cable channels. Therefore, achieving online monitoring and sensing of these faults and harmful gases is of paramount importance for the development of a resilient and secure power grid.

Since the mechanical exfoliation of graphene in 2004, the exploration of 2D materials has experienced a remarkable surge over the past 19 years, spanning various disciplines such as condensed matter physics, electronic engineering, and materials science.^{8–10} Starting with graphene, these two-dimensional materials have evolved into a diverse and expansive family characterized by their distinct structural features and physicochemical properties, progressively estab-

Received: October 26, 2023

Revised: February 1, 2024

Accepted: February 21, 2024

Published: April 1, 2024



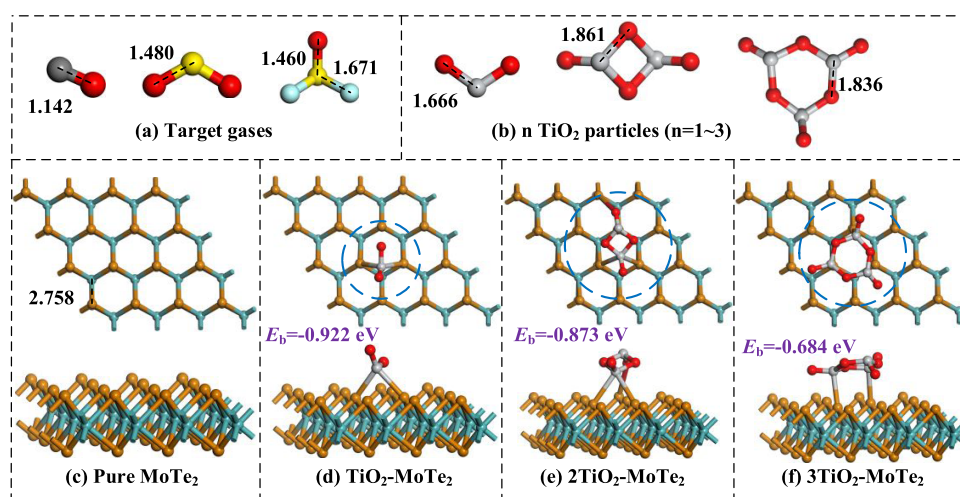


Figure 1. Optimized structures of (a) Target gases, (b) $n\text{TiO}_2$ particles ($n = 1-3$), (c) pure MoTe_2 , and (d-f) $n\text{TiO}_2$ particle ($n = 1-3$)-doped MoTe_2 .

lishing themselves as one of the most captivating categories of potential materials.^{11,12} However, due to graphene's inherent lack of a band gap and the absence of a straightforward method to induce one, researchers have progressively shifted their attention to other two-dimensional materials.

MoTe_2 , a constituent of the transition-metal dichalcogenide (TMD) family, has garnered significant attention from the academic community in recent years.¹³⁻¹⁵ MoTe_2 has gained prominence due to its robust spin-orbit coupling, diverse phase structures, exceptionally high charge carrier mobility, unsaturated magnetoresistance, and a rich interplay of nontrivial topological features and superconducting electronic states, positioning it at the forefront of materials for topological superconductivity and quantum computing research.^{16,17} Leveraging the exceptional electronic properties of MoTe_2 and its potential for adsorption and sensing.¹⁸⁻²⁰ Moreover, considering that monolayers of MoTe_2 exhibit similar features to other TMDs, such as MoS_2 and MoSe_2 , this similarity holds promise for favorable sensing characteristics.²¹⁻²⁴ This paper first considers the utilization of single-layer MoTe_2 for the detection and mitigation of faulty and hazardous gases within underground cable conduits, and this innovation holds the promise of enabling real-time monitoring of cables and faults, thereby contributing to the advancement of Internet-of-Things (IoT) technology.

Nanoparticle modification is one of the essential methods for enhancing the adsorption and sensing performance of materials,^{25,26} which has also been adopted in this work. Considering cost-effectiveness and preparation feasibility and given the outstanding performance of TiO_2 particles in material modification, TiO_2 particles were used as dopants. Additionally, taking into account the surface modification conditions in practical applications, this work incorporated dopant particle quantities ranging from one to three carefully selected based on the physical structure and adsorption performance of the adsorption system to investigate the most stable configurations. The band structures, total density of states (DOS), projected density of states (PDOS), differential charge density (DCD), and the molecular orbital theory of different adsorption systems were analyzed, further revealing the adsorption and sensing mechanisms of these gases on the TiO_2 particle-modified MoTe_2 monolayer. The findings of this article offer theoretical guidance for the development of

efficient and highly selective online monitoring sensors for underground cable channels, ensuring the stability and reliability of the power grid as well as the safety of cable operators.

2. COMPUTATIONAL DETAILS

The entire calculations in this work are based on density functional theory (DFT).^{27,28} Geometry optimization and energy calculations were performed by using the Dmol³ software package. Initially, a $4 \times 4 \times 1$ supercell of MoTe_2 was constructed comprising 16 Mo atoms and 32 Te atoms. Additionally, a vacuum space of 20 Å was built to mitigate the influence of neighboring unit cells.²⁹ Grimme referring to D3 was employed to treat vdW interactions.^{30,31} For structure optimization and energy calculations, a generalized gradient approximation (GGA) with the Perdew-Burke-Ernzerhof functional was employed to handle exchange-correlation electronic energy.^{32,33} Atomic orbitals were described using double numerical plus polarization (DNP), while the valence and core electrons were treated with density functional theory semicore pseudopotentials (DSSP).³⁴ Furthermore, given the electrical properties of MoTe_2 , no spin restriction was applied to the electronic spin. To perform geometry optimization and energy calculations for the supercell, a Monkhorst-Pack k-point grid of $8 \times 8 \times 1$ was defined, which is particularly suitable for 2D materials like MoTe_2 . To ensure computational accuracy, energy convergence tolerance, maximum force, and displacement were set to 10^{-6} Ha, 2×10^{-3} Ha/Å, and 5×10^{-3} Å, respectively, while the self-consistent field convergence precision was established at 10^{-6} Ha.³⁵ In addition, various initial configurations were explored and tested, and we selected the most stable structure by the magnitude of the adsorption energy. The global orbital cutoff radius was set at 5.0 Å. The binding energy (E_b), the adsorption energy (E_{ads}), the charge transfer (ΔQ), and E_g (energy gap) are defined as follows.³⁶

The binding energy (E_b) of $n\text{TiO}_2$ particle ($n = 1-3$)-doped MoTe_2 was calculated as

$$E_b = E_{X-\text{MoTe}_2} - E_X - E_{\text{MoTe}_2} \quad (1)$$

where $E_{X-\text{MoTe}_2}$, E_X and E_{MoTe_2} represent the total energy of $n\text{TiO}_2$ particle ($n = 1-3$)-doped MoTe_2 , isolated $n\text{TiO}_2$ particles ($n = 1-3$), and a pure MoTe_2 monolayer,

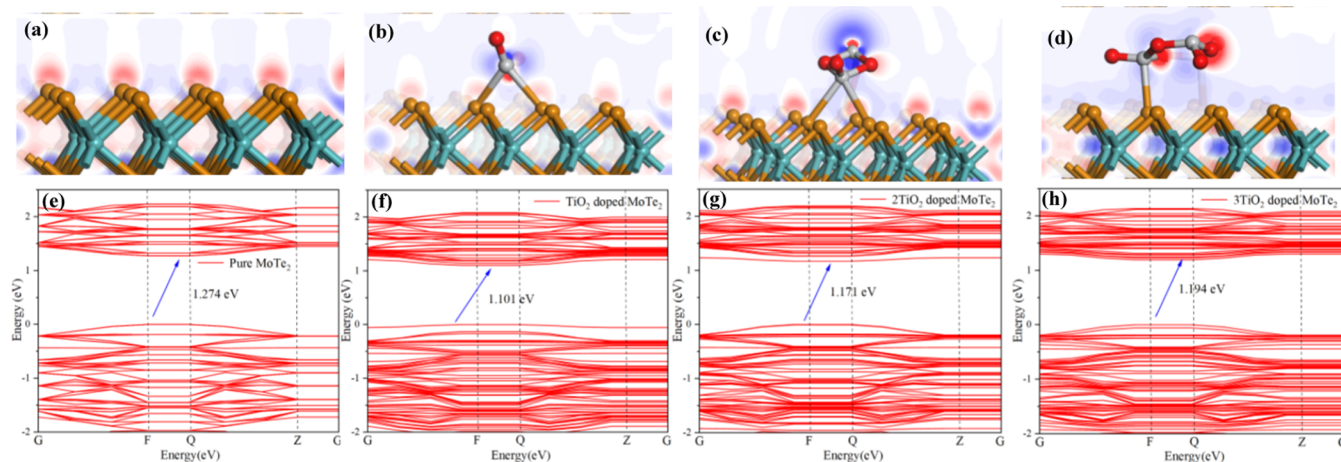


Figure 2. (a–d) Differential charge density (DCD) and (e–h) band structures of pure MoTe₂ and different doped systems.

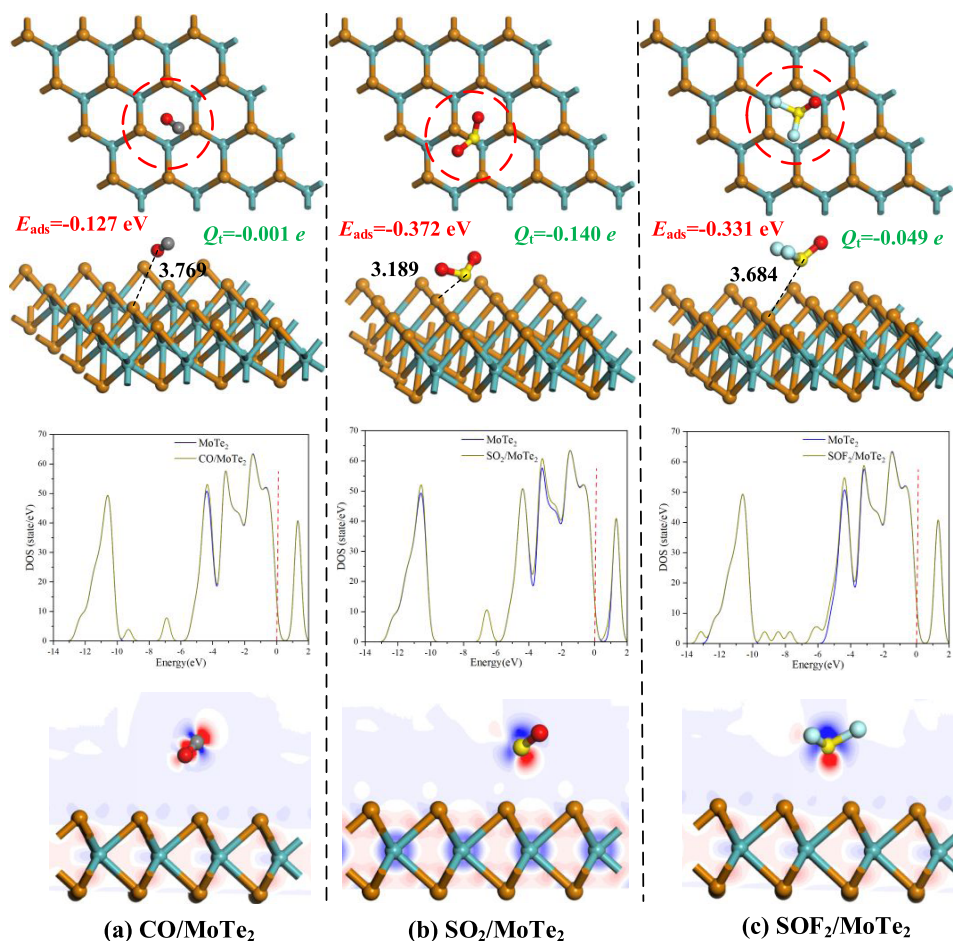


Figure 3. Most stable structures of faulty and hazardous gas adsorption on a pure MoTe₂ monolayer and differential charge density and density of states analysis of (a) CO/MoTe₂, (b) SO₂/MoTe₂, and (c) SOF₂/MoTe₂.

respectively. Higher binding energy indicates a more stable system.

The adsorption energy (E_{ads}) of surface reaction processes was calculated as

$$E_{\text{ads}} = E_{\text{gas}/X\text{-MoTe}_2} - E_{X\text{-MoTe}_2} - E_{\text{gas}} \quad (2)$$

where $E_{\text{gas}/X\text{-MoTe}_2}$, $E_{X\text{-MoTe}_2}$, and E_{gas} represent the total energy of the adsorbed system gas/ $n\text{TiO}_2\text{-MoTe}_2$ ($n = 1-3$), $n\text{TiO}_2$

particle ($n = 1-3$)-doped MoTe₂, and the isolated gas molecules, respectively.

The charge amount can be obtained through Millikan charge analysis, and the charge transfer (ΔQ) was defined by

$$\Delta Q = Q_a - Q_b \quad (3)$$

where Q_a and Q_b represent the charge of gases after and before adsorption, respectively.

3. RESULTS AND DISCUSSION

3.1. Optimized Structures and Electronic Property Analysis of Target Gases and a $n\text{TiO}_2$ Particle ($n = 1-3$)-Doped MoTe_2 Monolayer. In order to obtain the most stable doped structure, we perform structural optimizations of different doping sites by the above computational method, and Figure 1 shows the optimized structures and electronic property analysis of target gases and $n\text{TiO}_2$ particle ($n = 1-3$)-doped MoTe_2 . The figure illustrates that the CO molecule has a C–O bond length of 1.142 Å. In contrast, SO_2 exhibits a S–O bond length of 1.480 Å with sp^2 hybridization. It is worth noting that SOF_2 , a characteristic decomposition component of SF_6 under partial discharge conditions, is highly toxic. This compound has S–O and S–F bond lengths of 1.460 and 1.671 Å, respectively. Figure 1b depicts how an increasing number of TiO_2 particles tend to cluster, potentially forming stable cyclic cluster structures. In terms of the geometric structure, the intrinsic MoTe_2 structure offers a large specific surface area with numerous adsorption sites, making it highly capable of capturing fault gases in the cable channels. Figures 1d–f displays the top and side views of the most stable structure of a TiO_2 nanoparticle-doped MoTe_2 monolayer, with binding energies ($E_{\text{b,s}}$) of -0.922 , -0.873 , and -0.684 eV, respectively. These values indicate that an increase in the number of dopant particles decreases the stability of the entire doping system. Additionally, when dopants interact with the substrate surface, chemical bonds form, providing a stable support for gas adsorption.

Differential charge density (DCD) and band structures of pure MoTe_2 and different doped systems are shown in Figure 2a–h. For the interpretation of DCD, the red region represents an increase in electron density, while the green region represents a decrease in electron density, and the shade of color indicates the degree of charge aggregation. Meanwhile, the color map goes from -0.10 to 0.10 e/Å in this work. In addition, the calculation of the band structures can help in understanding the electronic properties of the modified material and assist in the development and utilization of gas sensors. According to the DCD analysis, it is evident that TiO_2 particle dopants function as electron acceptors, signifying that the primary electron transfer originates from the MoTe_2 surface toward the dopants. The calculated electron transfer values from Millikan charge analysis are -0.381 e, -0.392 e, and -0.598 e, implying the highest rate of electron migration when three TiO_2 particles are present. Furthermore, there is a conspicuous distinction in charge polarity within the doping region, indicating pronounced chemical reaction phenomena and thus underscoring the high stability and active electron attributes of the doping system. Band structure calculations unveil that the original MoTe_2 possesses a band gap of 1.274 eV. Postdoping, the band-gap values measure 1.101, 1.171, and 1.194 eV for varying quantities of TiO_2 nanoparticles. These changes exert a minimal influence on the energy level distribution with a decrease in the band gap of approximately 0.10 eV under different doping conditions. This effect can primarily be attributed to the reduced conduction band after particle doping. Collectively, the electron characteristics converge toward a common objective: TiO_2 particles have the potential to marginally enhance the band gap, diminish the electrical conductivity of the doping system, and heighten electron activity in the doping reaction zone, thereby facilitating gas capture.

3.2. Faulty and Hazardous Gas Adsorption on a Pure MoTe_2 Monolayer. Figure 3a–c illustrates the presentation of the most stable structures for the adsorption of faulty and hazardous gases on a MoTe_2 monolayer, along with the differential charge density and state density of the adsorption systems. In the figure, the adsorption distance is the closest distance between an atom in a gas molecule and a neighboring atom in the substrate. Integration of the adsorption data analysis and electronic properties reveals that the MoTe_2 monolayer demonstrates only a moderate adsorption capacity for these three target gases, primarily manifesting weak physical adsorption reactions. Geometric structure analysis suggests that gas molecules tend to adsorb at the center of the plane composed of three Te atoms on the MoTe_2 surface. The adsorption energies (E_{ads}) for the three systems, namely, CO/ MoTe_2 , SO_2 / MoTe_2 , and SOF_2 / MoTe_2 , are -0.127 , -0.372 , and -0.331 eV, with corresponding charge transfer quantities of -0.001 e, 0.140 e, and -0.049 e, respectively. The weak adsorption energy and the small amount of charge transfer prove that the intrinsic MoTe_2 has insufficient adsorption capacity for these target gases, and therefore, the sensitivity of gas detection is poor. Among these, CO adsorption exhibits the weakest capture effect, essentially suggesting weak physical interactions, while SO_2 adsorption outperforms the other two gases. The electron layer distribution of CO is more stable than that of the other two molecules; therefore, the gas adsorption is only physical and the charge transfer is quite small. Additionally, the adsorption distances for all three systems exceed 3 Å, maintaining a high level of consistency with other adsorption data, thus confirming the accuracy of the optimization results. From the distribution of the density of states (DOS), it can be observed that the reactivity of these gases on the MoTe_2 surface is minimal, with almost no significant impact on the electron distribution, except for a slight increase in electron density in the energy range from -6 eV to the Fermi level. Moreover, in the case of SO_2 adsorption, the charge density to the right of the Fermi level increases after gas adsorption, indicating an overall enhancement of the electrical conductivity for the entire adsorption system (Table 1).

Table 1. Adsorption Energy (E_{ads}), Charge Transfer (Q_{t}), and the Adsorption Distance (d) of the Pure MoTe_2 Monolayer

structure	figure	E_{ads} (eV)	Q_{t} (e)	d (Å)
CO/ MoTe_2	Figure 3a	-0.127	-0.001	3.769
SO_2 / MoTe_2	Figure 3b	-0.372	0.140	3.189
SOF_2 / MoTe_2	Figure 3c	-0.331	-0.331	3.684

DCD analysis reveals that gas molecules primarily function as electron acceptors during the surface action process, with the highest electron differential charge density observed in the case of SO_2 adsorption, aligning with the charge-transfer analysis results. Combining multidimensional structural and electronic property analyses, it can be inferred that the adsorption capacity of the pristine MoTe_2 monolayer is insufficient, and its detection ability for these faulty and hazardous gases has not yet reached the desired level.

3.3. Geometric Structures of CO, SO_2 , SOF_2 on $n\text{TiO}_2$ Particle ($n = 1-3$)-Doped MoTe_2 . In this section, various adsorption positions of the target gas on $n\text{TiO}_2$ particle ($n = 1-3$)-doped MoTe_2 surface were calculated, and the most

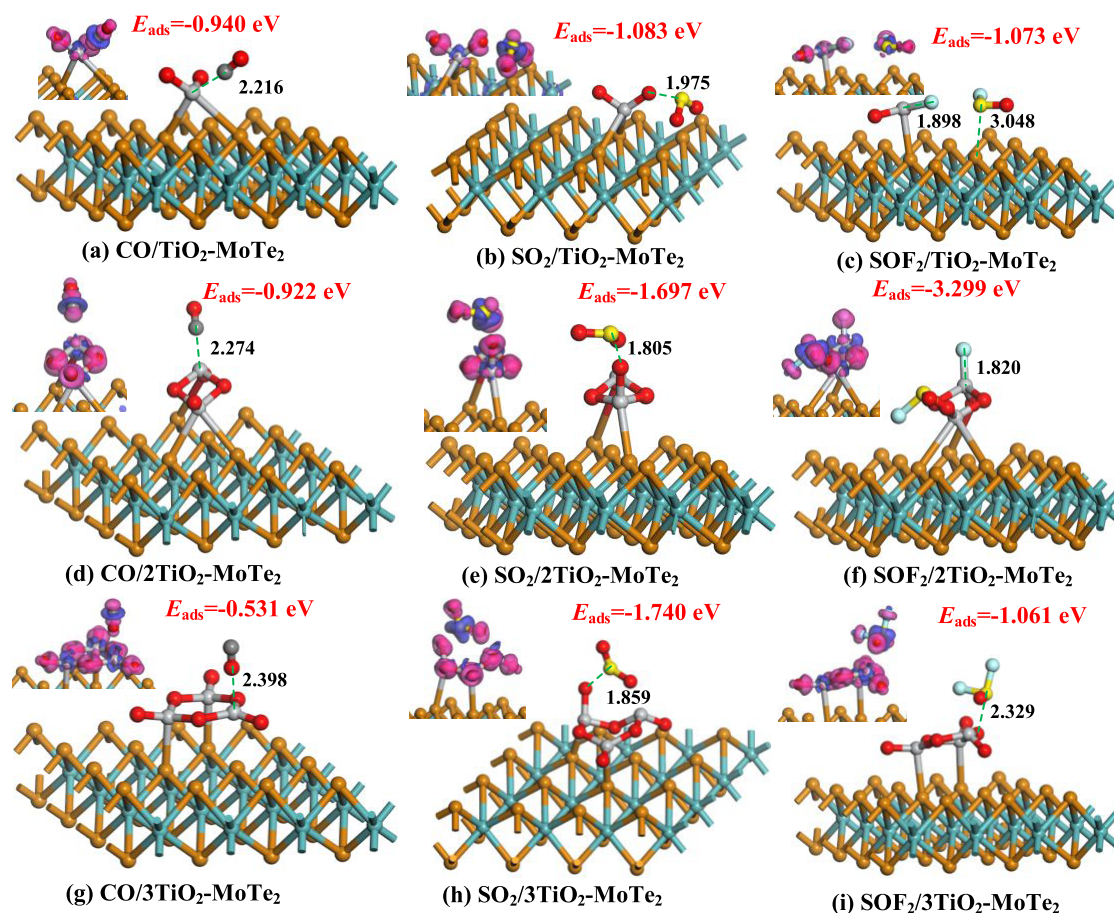


Figure 4. Geometric structures of CO, SO₂, and SOF₂ on the *n*TiO₂ particle (*n* = 1–3)-doped MoTe₂ monolayer.

stable adsorption structures under different doping scenarios, as shown in Figure 4a–i, were selected. After modification with a single TiO₂ nanoparticle, the adsorption performance was significantly enhanced, with adsorption energy at least three times higher than that of the original MoTe₂ monolayer. The adsorption energies for systems CO/TiO₂–MoTe₂, SO₂/TiO₂–MoTe₂, and SOF₂/TiO₂–MoTe₂ are –0.940, –1.083, and –1.073 eV, respectively, demonstrating competitive adsorption performance. It is worth noting that the adsorption of CO and SO₂ molecules results in minimal structural changes, indicating physisorption, while SOF₂ molecules undergo decomposition upon adsorption, forming independent F atoms and SOF groups bonded stably to TiO₂, suggesting chemisorption for SOF₂/TiO₂–MoTe₂. When two TiO₂ particles are doped, the adsorption strength exhibits a turning point, with the adsorption order being SOF₂ > SO₂ > CO, and the adsorption energy values decreasing in a stepwise manner, measuring –3.299, –1.697, and –0.922 eV, respectively. Compared to the first case, the CO molecule shifts from the dopant’s slanted position to the directly above position, while the SO₂ adsorption site changes from a horizontal position to above the dopant. Additionally, SOF₂ also undergoes decomposition, but the interaction strength is stronger than when a single TiO₂ modification is applied. In the three TiO₂-modified MoTe₂ adsorption systems, the CO adsorption system exhibits a noticeable decrease in adsorption energy, being only half of the first two adsorption scenarios. In contrast, the SO₂ adsorption performance reached its optimum value. Unfortunately, the adsorption capacity of SOF₂

significantly decreases. To better illustrate the electronic property changes before and after gas adsorption, we show the differential charge density in the upper left corner of the adsorption structures. It can be observed that only in the CO/TiO₂–MoTe₂ and CO/3TiO₂–MoTe₂ systems do the target gases act as electron donors, while in the other systems, the target gases act as electron acceptors, and the substrate modified by the dopant acts as an electron donor. From the values of charge transfer, SOF₂ exhibits the highest electron transfer due to chemisorption, and the electronic active region and stable region on the differential charge density are more visual. CO adsorption is primarily attributed to physisorption, resulting in a lower amount of electron transfer and a more gradual charge distribution. Compared to the Sc-doped MoTe₂, *n*TiO₂ particle doping improves the adsorption energy of SO₂ and SOF₂ by 30%.²⁰ In summary, the effect of TiO₂ nanoparticle dopants promotes the adsorption performance of original MoTe₂ and enhances the adsorption selectivity and sensitivity for these gases, facilitating the development and production of corresponding sensors (Table 2).

3.4. Electronic Properties of CO, SO₂, SOF₂ on *n*TiO₂ Particle (*n* = 1–3)-Doped MoTe₂. To further elucidate the adsorption and sensing mechanisms of the target gases on the MoTe₂ surface, the total density of states (DOS) of CO, SO₂, and SOF₂ adsorption on *n*TiO₂ particle (*n* = 1–3)-doped MoTe₂ is presented in Figure 5. Among the three CO adsorption systems, the influence of CO addition on DOS is almost negligible, especially in the cases of TiO₂ and 2TiO₂ doping, where the DOS before and after adsorption essentially

Table 2. Adsorption Energy (E_{ads}), Charge Transfer (Q_t), and the Adsorption Distance (d) of the $n\text{TiO}_2$ Particle ($n = 1-3$)-Doped MoTe_2 Monolayer

structure	figure	E_{ads} (eV)	Q_t (e)	d (Å)
$\text{CO}/\text{TiO}_2\text{-MoTe}_2$	Figure 4a	-0.940	0.180	2.216
$\text{SO}_2/\text{TiO}_2\text{-MoTe}_2$	Figure 4b	-1.083	-0.302	1.975
$\text{SOF}_2/\text{TiO}_2\text{-MoTe}_2$	Figure 4c	-1.073	-0.561	1.898
$\text{CO}/2\text{TiO}_2\text{-MoTe}_2$	Figure 4d	-0.922	-0.433	2.274
$\text{SO}_2/2\text{TiO}_2\text{-MoTe}_2$	Figure 4e	-1.697	-0.274	1.805
$\text{SOF}_2/2\text{TiO}_2\text{-MoTe}_2$	Figure 4f	-3.299	-0.529	1.820
$\text{CO}/3\text{TiO}_2\text{-MoTe}_2$	Figure 4g	-0.531	0.077	2.398
$\text{SO}_2/3\text{TiO}_2\text{-MoTe}_2$	Figure 4h	-1.740	-0.264	1.859
$\text{SOF}_2/3\text{TiO}_2\text{-MoTe}_2$	Figure 4i	-1.061	-0.025	2.329

overlap. However, when interacting with 3TiO_2 , a DOS peak near the Fermi level increases in the valence band region, attributed to electronic rearrangement after CO adsorption. In the case of SO_2 adsorption systems, the DOS of the adsorbed gas is mainly distributed in the -10 eV to Fermi level range. For $\text{SO}_2/\text{TiO}_2\text{-MoTe}_2$, after gas adsorption, the overall DOS

shifts slightly to the right, causing more electrons to transition from the valence band to the conduction band, ultimately resulting in an increase in the system's electrical conductivity. The $\text{SO}_2/2\text{TiO}_2\text{-MoTe}_2$ adsorption systems exhibit a similar trend, as the presence of SO_2 leads to a redistribution of electrons in the -5 to 0 and -17.5 to 15 eV energy level intervals. A significant DOS peak appears at the -16 eV energy level, while the distribution of electrons in the -5 to 0 eV range becomes more uniform. Due to chemical adsorption, the DOS of SOF_2 adsorption systems exhibits a broader distribution in the valence band region with multiple smaller DOS peaks. Additionally, charge migration near the Fermi level occurs, resulting in distinct changes in resistivity.

The distribution of projected density of states (PDOS) can effectively reveal the reasons for changes in the total density of states (DOS), as shown in Figure 6, which provides the PDOS for CO, SO_2 , and SOF_2 adsorption on $n\text{TiO}_2$ particle ($n = 1-3$)-doped MoTe_2 . The dashed line represents the Fermi level. It can be observed that the PDOS peaks of the CO adsorption system reach around 6 eV, which is the highest among these three adsorbed gases. However, due to the mild surface

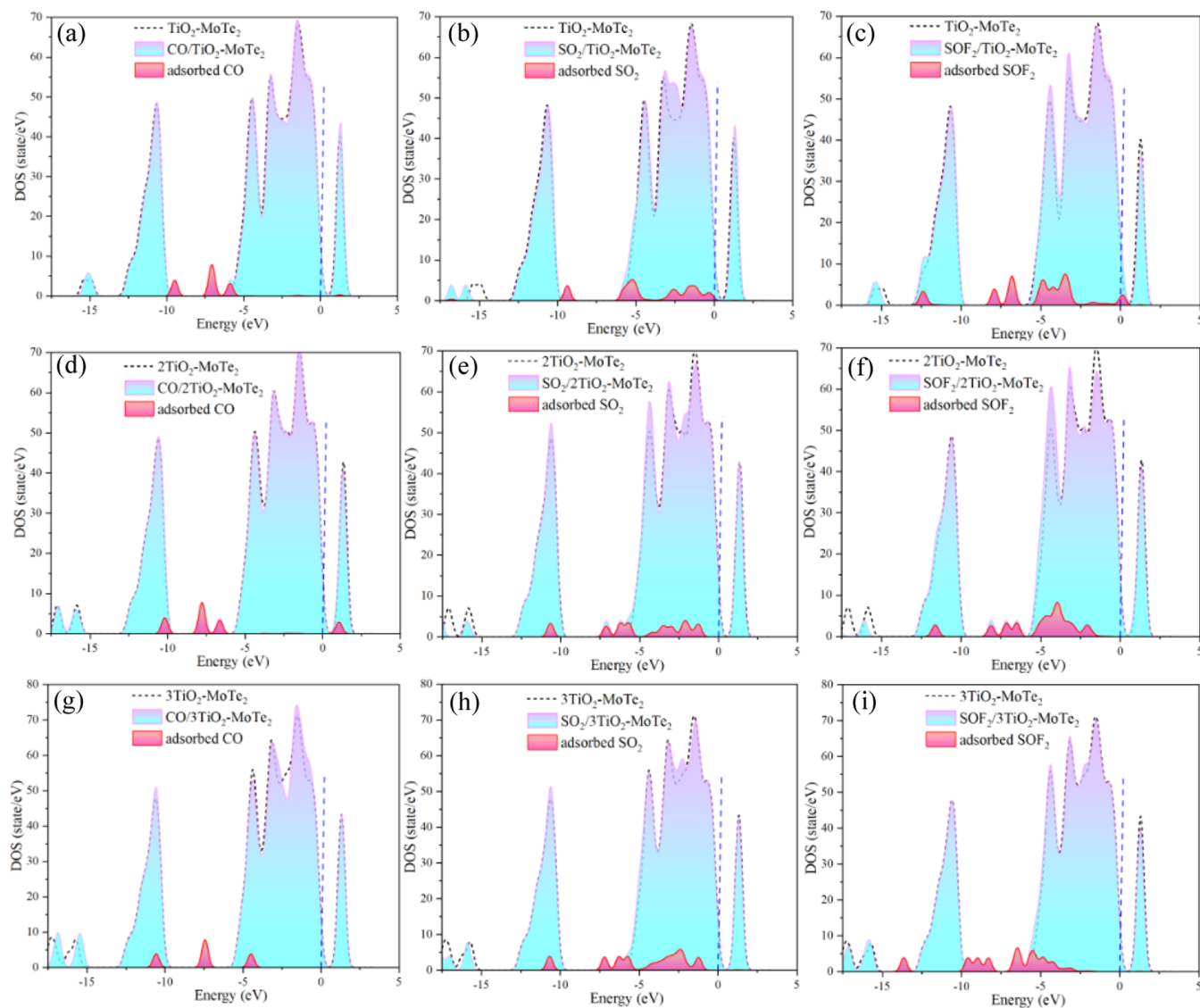


Figure 5. Total density of states of CO, SO_2 , SOF_2 on $n\text{TiO}_2$ particle ($n = 1-3$)-doped MoTe_2 .

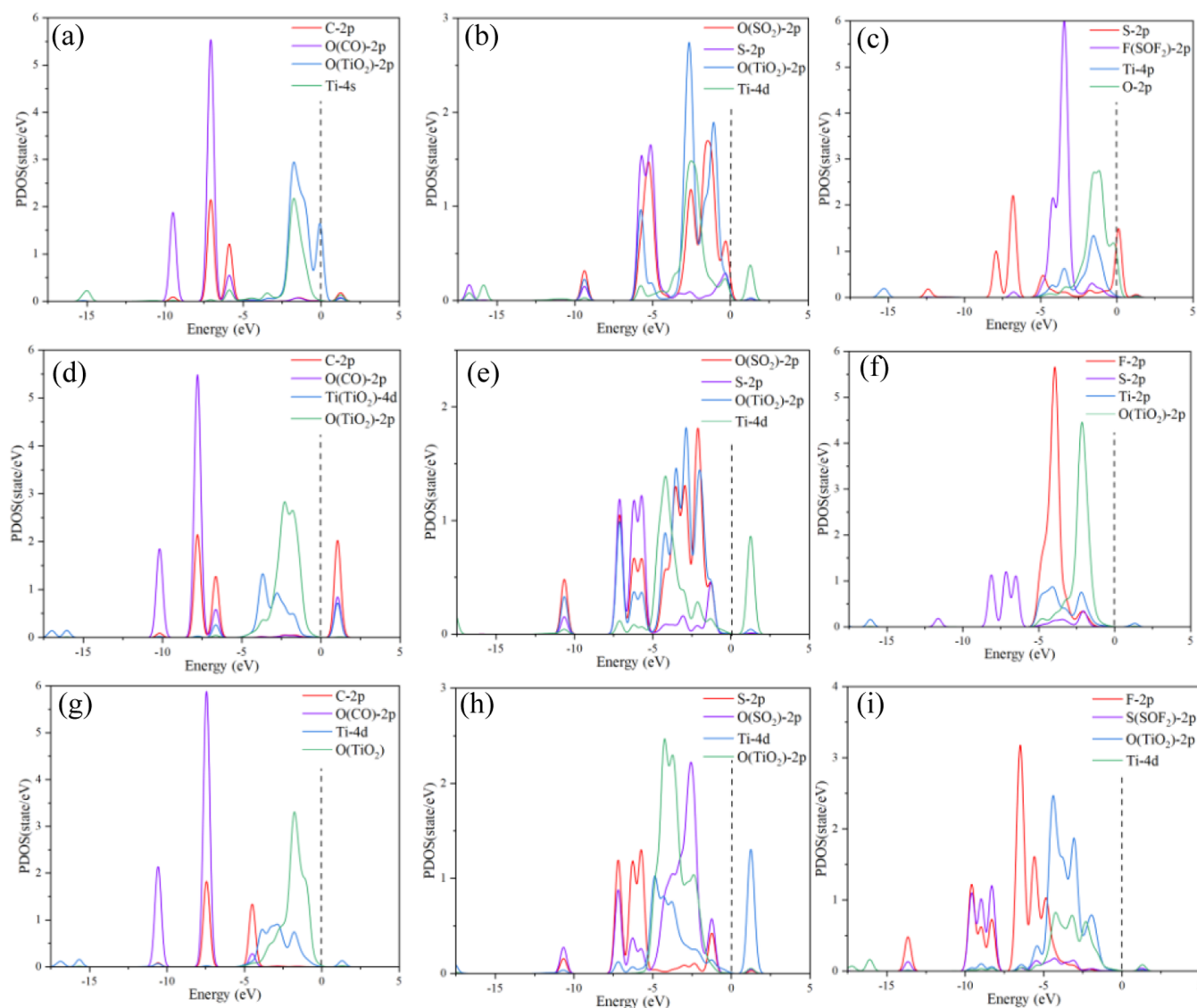


Figure 6. Projected density of states of CO, SO₂, SOF₂ on *n*TiO₂ particle (*n* = 1–3)-doped MoTe₂.

reaction, the PDOS is characterized by limited hybridization and orbital mixing. In this context, the 2p orbitals of the O atom play a predominant role in the adsorption process. Regarding SO₂ adsorption, there is significant hybridization between the 2p orbitals of the O atom, the 2p orbitals of the S atom, and the 4d orbitals of the Ti atom in the –10 to 0 eV range, resulting in prominent peaks at various energy levels. This phenomenon aligns with the adsorption behavior of SO₂. In the SOF₂ adsorption system, the 2p orbitals of the F atom make the most notable contribution, primarily attributed to the formation of Ti–F bonds during the adsorption process.

3.5. Theoretical Recovery Time and Band-Structure Analysis of the *n*TiO₂ Particle (*n* = 1–3)-Doped MoTe₂ Monolayer. The theoretical recovery time (τ) is one of the most crucial parameters that decides the superiority of the new gas-sensitive sensors.^{37,38} The theoretical recovery times of CO, SO₂, and SOF₂ are explored to assess the sensing capability and desorption effect of the *n*TiO₂ particle (*n* = 1–3)-doped MoTe₂ monolayer. The τ is defined in eq 4. Moreover, the calculation of the band structure facilitates the understanding of the conductive properties; thus, the band

structures are shown in Figure 7. The lower the band gap, the higher the conductivity.

$$\tau = \nu_0^{-1} \exp(-E_{\text{ads}}/K_{\text{B}}T) \quad (4)$$

In the above equation, *T* is temperature, the Boltzmann constant (*K_B*) is a physical constant with respect to temperature and energy, the value of *K_B* is 8.62 × 10^{–5} eV K^{–1}, and ν_0 is the attempt frequency. Moreover, we have several times calculated the attempt frequency for small molecules adsorbed on TMD surfaces, and indeed, in most cases, its value is on the order of 10¹² s^{–1}, and this conclusion is consistent with the findings of the existing literature.^{39,40}

The gas recovery time is one of the most characteristic indicators of sensor performance, so we calculated the theoretical gas recovery time for all target gases at room temperature and 373 K. At room temperature, the slowest τ of the three adsorption systems for CO is 7408.9 s, and the slowest τ of the three adsorption systems for SO₂ is 2.61 × 10¹⁷ s. Moreover, SOF₂ escapes the surface of *n*TiO₂ particle (*n* = 1–3)-doped MoTe₂ and requires a minimum of 8.67 × 10⁵. When the temperature reaches 100 °C, the τ of CO/*n*TiO₂–MoTe₂ systems is 4.80 s, 2.75 s, and 1.46 × 10^{–5} s, and the τ of

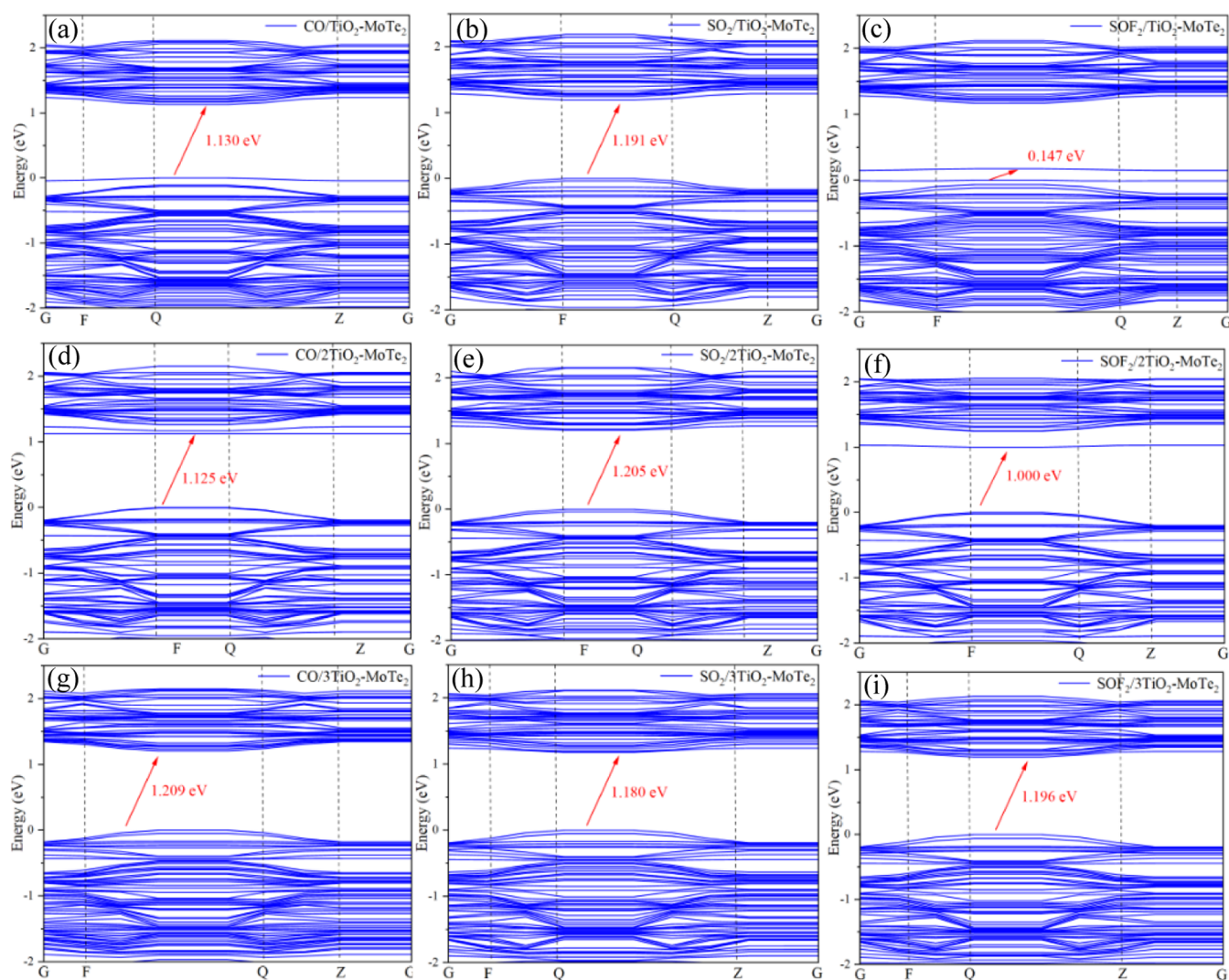


Figure 7. Band structures of CO, SO₂, and SOF₂ on *n*TiO₂ particle (*n* = 1–3)-doped MoTe₂.

SO₂/*n*TiO₂–MoTe₂ systems is 408.74 s, 7.86×10^{12} s, and 2.99×10^{12} s; at last, the τ of SOF₂/*n*TiO₂–MoTe₂ systems is 299.59 s, 3.22×10^{32} s, and 206.36 s. In addition, the increase in ambient temperature results in a significant decrease in gas recovery time, and according to our calculations, ideal desorption can be achieved at temperatures above 100 °C. This result indicates that CO adsorption can achieve an ideal recovery time, which is favorable for recycling of the sensor, while SO₂ and SOF₂ can achieve ideal gas recovery characteristics under some specific conditions, which is more suitable for the adsorption of these two harmful gases. The band-structures analysis shows that CO adsorption leads to a small increase in the energy gap value, 1.101–1.130, 1.125, and 1.209 eV in three adsorption regimes, resulting in a decrease in the conductivity of the whole system. The SO₂ adsorption scenario keeps the energy gap value almost constant, whereas SOF₂ causes a decrease in the energy gap value. Such different trends are effective for the sensing and monitoring of these target gases.

4. CONCLUSIONS

In this paper, the adsorption mechanism and electrical properties of the *n*TiO₂ particle (*n* = 1–3)-doped MoTe₂ monolayer to faulty and hazardous gases in the underground

cableway were first explored based on density functional theory. The band structure, total density of states, projected density of states, and differential charge density were analyzed, and the primary conclusions are as follows:

- (1) TiO₂ particles have the potential to marginally enhance the band gap, diminish the electrical conductivity of the doping system, and heighten electron activity in the doping reaction zone, thereby facilitating gas capture.
- (2) The best adsorption performance was achieved in the case of two-particle doping. Furthermore, the modified MoTe₂ exhibits an enhanced capability for capturing SO₂ and SOF₂, with the adsorption mechanism classified as physical–chemical adsorption.
- (3) Significant differences in DOS and PDOS occur for different adsorption systems; this is attributed to the differences in electronic properties under different adsorption types.
- (4) Calculation of theoretical recovery time indicates that CO adsorption can achieve ideal recovery time, which is favorable for recycling of the sensor, while SO₂ and SOF₂ can achieve ideal gas recovery characteristics under some specific conditions, which is more suitable for the adsorption of these two harmful gases.

This work not only introduces a novel surface modification method for the MoTe₂ monolayer but also provides a substantial data set to support the design and production of efficient sensors used in the underground cableway.

AUTHOR INFORMATION

Corresponding Author

Jipeng Mei – China Three Gorges University, Yichang 443000
Hubei, China; orcid.org/0009-0001-3822-9607;
Email: xslw1234@outlook.com

Author

Ziwen Yu – China Three Gorges University, Yichang 443000
Hubei, China

Complete contact information is available at:

<https://pubs.acs.org/10.1021/acsomega.3c08469>

Author Contributions

J.M. contributed to methodology; software; investigation; writing—original draft, review, and editing; conceptualization; funding acquisition; validation; and resources. Z.Y. contributed to validation, resources, software, and investigation.

Notes

The authors declare no competing financial interest.

ACKNOWLEDGMENTS

This work was supported financially by the National Natural Science Foundation of China (Grant No. 52107108).

REFERENCES

- (1) Buchholz, V.; Colwell, M.; Orton, H. E.; Wong, J. Y. ELEVATED-TEMPERATURE OPERATION OF XLPE DISTRIBUTION CABLE SYSTEMS. *IEEE Trans. Power Delivery* **1993**, *8*, 743–749.
- (2) Lux, J.; Olschewski, M.; Schäfer, P.; Hill, W. Real-Time Determination of Depth of Burial Profiles for Submarine Power Cables. *IEEE Trans. Power Delivery* **2019**, *34*, 1079–1086.
- (3) Zhou, W. Q.; Cheng, H.; Hui, B. J.; Huang, J. S.; Hao, Y. P.; Liu, G.; Li, L. C. Key process of the deflection of PET buffer layer in XLPE power cable by a case study: Thermo-oxidative degradation. *Eng. Failure Anal.* **2023**, *146*, No. 107131.
- (4) Cheetham, P.; Al-Taie, A.; Telikapalli, S.; Stamm, T.; Kim, C. H.; Graber, L.; Pamidi, S. Development of a High-Temperature Superconducting Gas-Insulated Power Cable. *IEEE Trans. Appl. Supercond.* **2020**, *30*, No. 7700207.
- (5) Li, T.; Gui, Y. G.; Zhao, W. H.; Tang, C.; Dong, X. C. Palladium modified MoS₂ monolayer for adsorption and scavenging of SF₆ decomposition products: A DFT study. *Phys. E* **2020**, *123*, No. 114178.
- (6) Sun, H.; Tao, L. Q.; Li, T.; Gao, X.; Sang, T. Y.; Li, Y. B.; Wei, Y. G.; Wang, G. Y.; Peng, Z. R.; Gui, Y. G.; Xia, S. Y.; Li, J. TiO₂-Doped GeSe Monolayer: A highly selective gas sensor for SF₆ decomposed species detection based on DFT method. *Appl. Surf. Sci.* **2022**, *572*, No. 151212.
- (7) Ammar, H. Y.; Badran, H. M. Effect of CO adsorption on properties of transition metal doped porphyrin: A DFT and TD-DFT study. *Heliyon* **2019**, *5*, No. e02545.
- (8) Wang, J. F.; Jin, X. X.; Li, C. H.; Wang, W. J.; Wu, H.; Guo, S. Y. Graphene and graphene derivatives toughening polymers: Toward high toughness and strength. *Chem. Eng. J.* **2019**, *370*, 831–854.
- (9) Wang, Y.; Li, S. S.; Yang, H. Y.; Luo, J. Progress in the functional modification of graphene/graphene oxide: a review. *RSC Adv.* **2020**, *10*, 15328–15345.
- (10) Edwards, R. S.; Coleman, K. S. Graphene synthesis: relationship to applications. *Nanoscale* **2013**, *5*, 38–51.
- (11) Schwierz, F.; Pezoldt, J.; Granzner, R. Two-dimensional materials and their prospects in transistor electronics. *Nanoscale* **2015**, *7*, 8261–8283.
- (12) Burch, K. S.; Mandrus, D.; Park, J. G. Magnetism in two-dimensional van der Waals materials. *Nature* **2018**, *563*, 47–52.
- (13) Xu, X. L.; Pan, Y.; Liu, S.; Han, B.; Gu, P. F.; Li, S. H.; Xu, W. J.; Peng, Y. X.; Han, Z.; Chen, J.; Gao, P.; Ye, Y. Seeded 2D epitaxy of large-area single-crystal films of the van der Waals semiconductor 2H MoTe₂. *Science* **2021**, *372*, 195–200.
- (14) Wu, D.; Guo, C. G.; Zeng, L. H.; Ren, X. Y.; Shi, Z. F.; Wen, L.; Chen, Q.; Zhang, M.; Li, X. J.; Shan, C. X.; Jie, J. S. Phase-controlled van der Waals growth of wafer-scale 2D MoTe₂ layers for integrated high-sensitivity broadband infrared photodetection. *Light: Sci. Appl.* **2023**, *12*, No. 5.
- (15) Zhang, C. X.; Gong, C.; Nie, Y. F.; Min, K. A.; Liang, C. P.; Oh, Y. J.; Zhang, H. J.; Wang, W. H.; Hong, S.; Colombo, L.; Wallace, R. M.; Cho, K. Systematic study of electronic structure and band alignment of monolayer transition metal dichalcogenides in Van der Waals heterostructures. *2D Mater.* **2017**, *4*, No. 015026.
- (16) Zhou, L.; Xu, K.; Zubair, A.; Liao, A. D.; Fang, W. J.; Ouyang, F. P.; Lee, Y. H.; Ueno, K.; Saito, R.; Palacios, T.; Kong, J.; Dresselhaus, M. S. Large-Area Synthesis of High-Quality Uniform Few-Layer MoTe₂. *J. Am. Chem. Soc.* **2015**, *137*, 11892–11895.
- (17) Ruppert, C.; Aslan, O. B.; Heinz, T. F. Optical Properties and Band Gap of Single- and Few-Layer MoTe₂ Crystals. *Nano Lett.* **2014**, *14*, 6231–6236.
- (18) Liu, Y. J.; Ren, M.; Song, B.; Dong, M. A DFT study of toxic gases (NH₃, C₂H₂, NO) adsorption and detection on metal oxides (CuO, Ag₂O, In₂O₃) modified MoTe₂ monolayer. *Appl. Surf. Sci.* **2023**, *622*, No. 156858.
- (19) Jiang, T. Y.; Zhang, W. T.; Zhang, T.; Yuan, H. X.; Bi, M. Q.; Zhou, X. Adsorption and gas-sensing performances of C₂H₂, C₂H₄, CO, H₂ in transformer oil on Pt-doped MoTe₂ monolayer: A DFT study. *Phys. E* **2023**, *146*, No. 115568.
- (20) Shi, Z. Y.; Zhang, Y.; Zeng, W.; Zhou, Q. A DFT study on adsorption of SF₆ decomposition gases (H₂S, SO₂, SO₂F₂ and SOF₂) on Sc-MoTe₂ monolayer. *Sens. Actuators, B* **2023**, *360*, No. 114548.
- (21) Baek, J.; Yin, D. M.; Liu, N.; Omkaram, I.; Jung, C.; Im, H.; Hong, S.; Kim, S. M.; Hong, Y. K.; Hur, J.; Yoon, Y.; Kim, S. A highly sensitive chemical gas detecting transistor based on highly crystalline CVD-grown MoSe₂ films (vol 10, pg 1861, 2017). *Nano Res.* **2017**, *10*, 2904.
- (22) Kumar, R.; Goel, N.; Kumar, M. UV-Activated MoS₂ Based Fast and Reversible NO₂ Sensor at Room Temperature. *ACS Sens.* **2017**, *2*, 1744–1752.
- (23) Wu, E. X.; Xie, Y.; Yuan, B.; Zhang, H.; Hu, X. D.; Liu, J.; Zhang, D. H. Ultrasensitive and Fully Reversible NO₂ Gas Sensing Based on p-Type MoTe₂ under Ultraviolet Illumination. *ACS Sens.* **2018**, *3*, 1719–1726.
- (24) Pham, T.; Li, G. H.; Bekyarova, E.; Itkis, M. E.; Mulchandani, A. MoS₂-Based Optoelectronic Gas Sensor with Sub-parts-per-billion Limit of NO₂ Gas Detection. *ACS Nano* **2019**, *13*, 3196–3205.
- (25) Li, T.; Hu, S. L.; Ma, R.; Sang, T. Y.; Chen, Q. L.; Ma, L.; Chen, Y.; Liao, Y.; Yang, G. L.; Huang, Y. F.; Deng, Y.; Jiang, X. L. The electronic properties and adsorption mechanism of Ag_n, Au_n (n = 1–4) modified GeSe monolayer towards hazardous gases (H₂S, NH₃, NO₂ and SOF₂): A first-principles study. *Surf. Interfaces* **2022**, *32*, No. 102150.
- (26) Gui, Y. G.; Li, T.; He, X.; Ding, Z. Y.; Yang, P. G. Pt Cluster Modified h-BN for Gas Sensing and Adsorption of Dissolved Gases in Transformer Oil: A Density Functional Theory Study. *Nanomaterials* **2019**, *9*, 1746.
- (27) Kim, M. C.; Sim, E.; Burke, K. Understanding and Reducing Errors in Density Functional Calculations. *Phys. Rev. Lett.* **2013**, *111*, No. 073003.
- (28) Medvedev, M. G.; Bushmarinov, I. S.; Sun, J. W.; Perdew, J. P.; Lyssenko, K. A. Density functional theory is straying from the path toward the exact functional. *Science* **2017**, *355*, 49–52.

- (29) Liu, H. C.; Tan, Z. X.; Niu, Y. X.; Wang, S. G.; Wang, Y. Ir-decorated MoS₂ monolayer as a promising candidate to detect dissolved gas in transformer oil: A DFT study. *Chem. Phys. Lett.* **2023**, *818*, No. 140410.
- (30) Lin, Y. S.; Li, G. D.; Mao, S. P.; Chai, J. D. Long-Range Corrected Hybrid Density Functionals with Improved Dispersion Corrections. *J. Chem. Theory Comput.* **2013**, *9*, 263–272.
- (31) Wang, Y.; Li, T.; Peng, Y. J.; Gui, Y. G.; Sun, H. Pd and Pt decorated GeSe monolayers as promising materials for SOF₂ and SO₂F₂ sensing. *Appl. Surf. Sci.* **2021**, *560*, No. 150028.
- (32) Furness, J. W.; Kaplan, A. D.; Ning, J. L.; Perdew, J. P.; Sun, J. W. Accurate and Numerically Efficient r²SCAN Meta-Generalized Gradient Approximation. *J. Phys. Chem. Lett.* **2020**, *11*, 8208–8215.
- (33) An, X. Y.; Guo, L.; Li, A. X. A DFT Study of the CO Oxidation Mechanism on Al_nAu (n = 1–12) Clusters. *J. Cluster Sci.* **2015**, *26*, 505–527.
- (34) Li, T.; Pan, S. X.; Ma, R.; Sang, T. Y.; Ma, L.; Wang, M. Z.; Zeng, W.; Huang, W. H.; Jiang, X. L.; Yang, G. L. The gas sensing and adsorption properties of XO₂ (X = Ti, Zr, Hf) doped C₃N towards H₂S, SO₂, SOF₂: A first-principles study. *Diamond Relat. Mater.* **2022**, *130*, No. 109553.
- (35) He, X.; Gui, Y. G.; Xie, J. F.; Liu, X.; Wang, Q.; Tang, C. A DFT study of dissolved gas (C₂H₂, H₂, CH₄) detection in oil on CuO-modified BNNT. *Appl. Surf. Sci.* **2020**, *500*, No. 144030.
- (36) Li, P.; Hong, Q. Y.; Wu, T.; Cui, H. SOF₂ sensing by Rh-doped PtS₂ monolayer for early diagnosis of partial discharge in the SF₆ insulation device. *Mol. Phys.* **2021**, *119*, No. e1919774.
- (37) Peng, S.; Cho, K. J.; Qi, P. F.; Dai, H. J. Ab initio study of CNT NO₂ gas sensor. *Chem. Phys. Lett.* **2004**, *387*, 271–276.
- (38) Szary, M. J. Computational study of the intercalation of NO₂ between bilayer MoTe₂. *Appl. Surf. Sci.* **2023**, *611*, No. 155514.
- (39) Cui, H.; Zhang, X. X.; Zhang, G. Z.; Tang, J. Pd-doped MoS₂ monolayer: A promising candidate for DGA in transformer oil based on DFT method. *Appl. Surf. Sci.* **2019**, *470*, 1035–1042.
- (40) Liu, H.; Xu, L. N.; Gui, Y. G.; Ran, L.; Chen, X. P. Adsorption properties of Ag₂O-MoSe₂ towards SF₆ decomposed products. *Vacuum* **2021**, *189*, No. 110248.